*Chapter 5*

# Hysteresis Model

## 5.1 General

The hysteresis model developed in this chapter embodies the core of the multiple-bolt model. It is later integrated into a stiffness model which accounts for the force-displacement interaction among the bolts (Figure 5.1). The model derived here 'smears' local differences in properties surrounding the bolt (embedment strength and stiffness) into an equivalent system.

The force-displacement interaction of the individual bolts is obtained by a spring model:

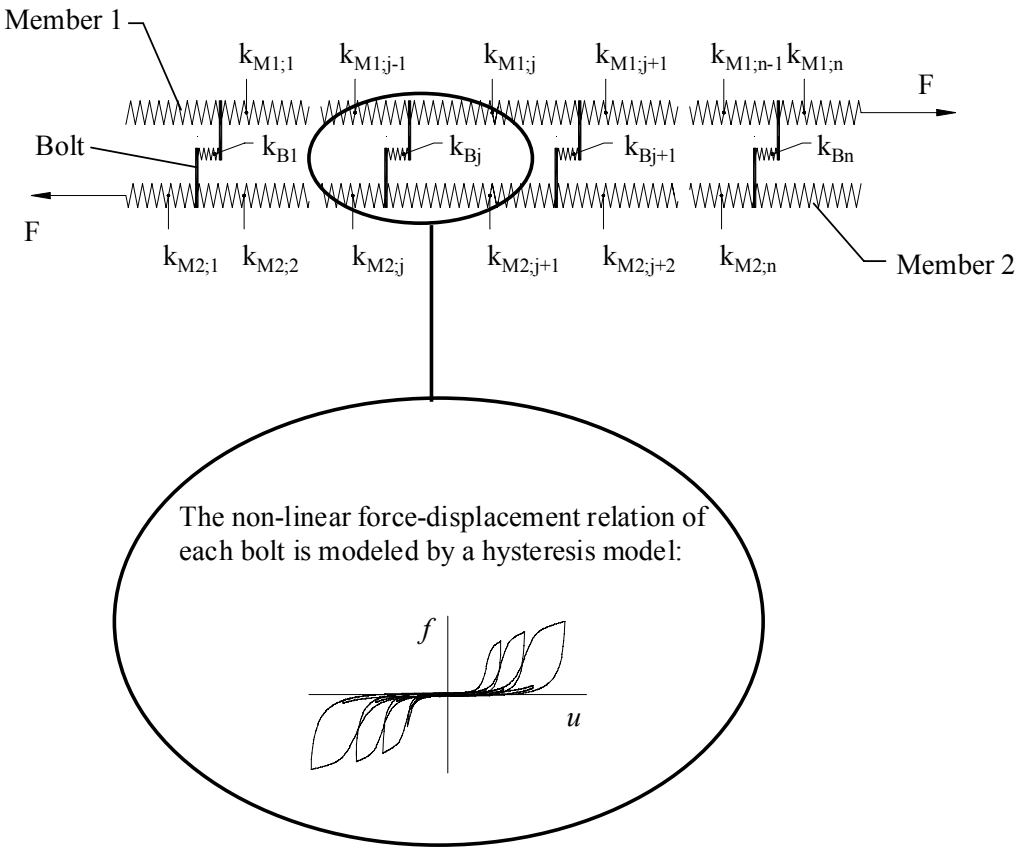


Figure 5.1: Modeling approach. Members are modeled with linear elastic springs. All nonlinear effects are modeled with the hysteresis model.

The objective is to develop a hysteresis model that is generic, computationally efficient, and mathematically traceable such that it is applicable to random input functions such as earthquake records. The basis for the model derived in this chapter is the hysteresis model put forth by Bouc, Wen, Baber and Noori (Baber and Noori 1986). However, to incorporate slack, reduce the dependency on energy dissipation, make it applicable to multiple fastener joints, and reduce the number of parameters that need to be identified, the BWBN model was significantly modified. The result is a new hysteresis model that explains the hysteresis of slack systems. The model is part of the MULTBOLT computer program developed in this work, which was written in FORTRAN and computes the response of multiple-bolt joints of various configurations subjected to cyclic excitation.

## 5.2 Model Development

The hysteretic behavior of the of each bolt is modeled as a single-degree-of-freedom system since there is only one moving mass (side member plus fixture and machine head in case of isolated laboratory tests, Figure 5.2). Note that this only applies to the hysteresis model. MULTBOLT is a multi-degree-of-freedom model (e.g. displacement of mass per bolt, slack increase, member strain, etc.). In the hysteresis model, each bolt is modeled separately and then incorporated into a structural model which is described in Chapter 7.

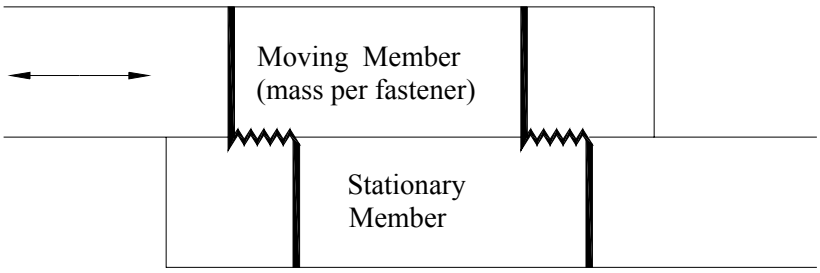


Figure 5.2: Single degree of freedom system

The solution of the simulated vibrating system is proportional to its mass. Therefore, to simplify computation, it is assumed that the mass per fastener is one unit. At slowly changing displacement rates, the determination of the mass is immaterial since practically no acceleration exists. At more erratic displacement rates that trigger inertia effects, the solution can be easily scaled by the measured mass of the system.

The basis of the model derived in this chapter, and the BWBN model, is the equation of motion for a single degree of freedom system consisting of a mass connected in parallel to a

viscous damper, a linear spring and a non-linear, hysteretic spring. Hence, the equation of motion of such a system may be described as[1]

$$\ddot{u}(t) + 2 \cdot \xi_0 \cdot \omega \cdot \dot{u}(t) + \mathrm{H}(u,z,t) = f(t) \tag{5.1}$$

where the total restoring force *H,* which is composed of both linear and hysteretic restoring forces, is given by

$$\mathrm{H}(u,z,t) = f_R(u,t) + f_h(z,t) = \alpha \cdot \omega^2 \cdot u(t) + (1-\alpha) \cdot \omega^2 \cdot z(t) \tag{5.2}$$

| | | Unit[2] |
|---|---|---|
| $f_R$ | linear restoring force (mass normalized) | kN/kg |
| $f_h$ | hysteretic force (mass normalized) | kN/kg |
| $\omega$ | pseudo-natural frequency of the non-linear system | rad/sec $10^6$ |
| *f(t)* | force function (mass normalized) | kN/kg |
| *t* | time | sec |
| $\xi$ | linear elastic viscous damping ratio | |
| *u* | total displacement of the mass, *m* | mm |
| *z* | hysteretic displacement | mm |
| $\alpha$ | rigidity ratio | |

Although all elements are arranged in parallel, the non-linear restoring force is a function of the fictitious hysteretic displacement, *z*, rather than total displacement, *u*. The reason behind this is to enable variation of the total contribution of the non-linear restoring force to the overall force. The relative input of the hysteretic part is therefore controlled by the parameter $\alpha$ with

$$0 \le \alpha \le 1.0 \tag{5.3}$$

In other words, a highly non-linear system such as a nailed joint in wood loaded perpendicular to the grain has a relatively small $\alpha$, whereas a linear spring mass-damper system has an $\alpha$ equal to 1.0. For $\alpha = 0$, the system is completely non-linear.

### 5.2.1 The Hysteresis

The hysteretic displacement, *z*, is a function of the hysteretic force. A hysteresis may be obtained by varying the hysteretic displacement, *z*, with *u* in a rate-type manner. That is *z* varies

[1] Normalized by mass divided by number of fasteners.

[2] All units in this chapter are specified as used in MULTBOLT.

with $u$ at different rates depending on direction of movement (positive or negative velocity) and displacement level. For example, an elliptic hysteresis is obtained if $z$ increases more rapidly at small negative $u$ and positive velocity and decreases more rapidly at large positive $u$ and negative velocity. At larger displacements, for a non-pinching, non-degrading system, the BWBN model expresses $z$ in form of the differential Equation

$$\dot{z}(t) = A \cdot \dot{u}(t) - \left(\beta \cdot |\dot{u}(t)| \cdot |z(t)|^{n-1} \cdot z(t) + \gamma \cdot \dot{u}(t) \cdot |z(t)|^{n}\right) \tag{5.4}$$

| | | Unit |
|---|---|---|
| $u$ | total displacement of the mass, $m$ | mm |
| $z$ | hysteretic displacement | mm |
| $A$ | parameter controlling hysteresis amplitude | |
| $\beta, \gamma, n$ | parameters describing shape and amplitude of hysteresis $1.0 \leq n$ | |

As can be readily observed from Equation (5.4), the parameter $A$ directly influences the variation of $z$ with time. Hence, $A$ controls hysteretic stiffness. In addition, $A$ dictates the hysteretic displacement amplitude $z_{max}$. To see this, consider that the hysteresis is described by a continuous function and the hysteretic stiffness is always zero at the local maximum or minimum, which is the point on the load-slip curve where the velocity changes sign. Therefore, at an infinitesimal small distance $dz$ away from $z_{max}$, where the velocity is close to but not equal to zero and where $z \neq z_{max}$ it must be true that

$$\dot{z}_{\max} \approx 0 = A \cdot \dot{u}(t) - \left(\beta \cdot |\dot{u}(t)| \cdot |z_{\max}|^{n-1} \cdot z_{\max} + \gamma \cdot \dot{u}(t) \cdot |z_{\max}|^{n}\right) \tag{5.5}$$

It follows

$$z_{\max} = \pm\left(\frac{A}{\beta + \gamma}\right)^{\frac{1}{n}} \tag{5.6}$$

For greater versatility $A$ may be varied with dissipated energy or any other measure that seams appropriate. Although the inclusion of parameter $A$ grants increased versatility of the BWBN model, $A$ is somewhat redundant in light of the fact that both hysteretic stiffness as well as the maximum influence of the hysteretic force, which in turn is a function of the hysteretic displacement amplitude, can be varied by the rigidity ratio $\alpha$, the parameters $\beta$, $\gamma$, $n$, and

degradation parameters, respectively. Thus, henceforth $A$ will be set equal to 1.0 and the non-degrading non-pinching hysteresis is now described as

$$\dot{z}(t) = \dot{u}(t) - \left(\beta \cdot \left|\dot{u}(t)\right| \cdot \left|z(t)\right|^{n-1} \cdot z(t) + \gamma \cdot \dot{u}(t) \cdot \left|z(t)\right|^{n}\right) \tag{5.7}$$

*5.2.1.1 Hysteresis Shape Parameters*

The three hysteresis shape parameters, $\beta$, $\gamma$, $n$, and their interaction, determine the basic shape of the hysteresis. The model is relatively insensitive to the *absolute* values of $\beta$ and $\gamma$ if both are changed proportionally, though very large values (absolute values > 50.0) of both parameters tend to cause significant numeric noise. Absolute values of $\beta$ and $\gamma$ inversely influence hysteretic stiffness and strength, as well as the smoothness of the hysteresis loop. However, the magnitude of influence is quite small. Great sensitivity exists as to the *relative* value of $\beta$ with respect to $\gamma$ and vice versa. The combination of $\beta$ and $\gamma$ dictates whether the model describes a hardening or softening load-slip relationship (Figure 5.3). For $n$ = 1.0, Baber (1980) listed the following relationships between $\beta$ and $\gamma$ and their effects on the hysteresis:

$$\left.\begin{aligned}\beta + \gamma &> 0.0\\ \gamma - \beta &< 0.0\end{aligned}\right\}$$ Weak softening (5.8)

$$\left.\begin{aligned}\beta + \gamma &> 0.0\\ \gamma - \beta &= 0.0\end{aligned}\right\}$$ Weak softening on loading, mostly linear unloading (5.9)

$$\left.\begin{aligned}\beta + \gamma &> \beta - \gamma\\ \beta - \gamma &> 0.0\end{aligned}\right\}$$ Strong softening loading and unloading, narrow hysteresis (5.10)

$$\left.\begin{aligned}\beta + \gamma &= 0.0\\ \gamma - \beta &< 0.0\end{aligned}\right\}$$ Weak hardening (5.11)

$$\left.\begin{aligned}0.0 &> \beta + \gamma\\ \beta + \gamma &> \gamma - \beta\end{aligned}\right\}$$ Strong hardening (5.12)

Based on this research and work reported by Foliente (1993), the condition expressed in Equation (5.8) yields hystereses that most closely resemble test data of timber structures.

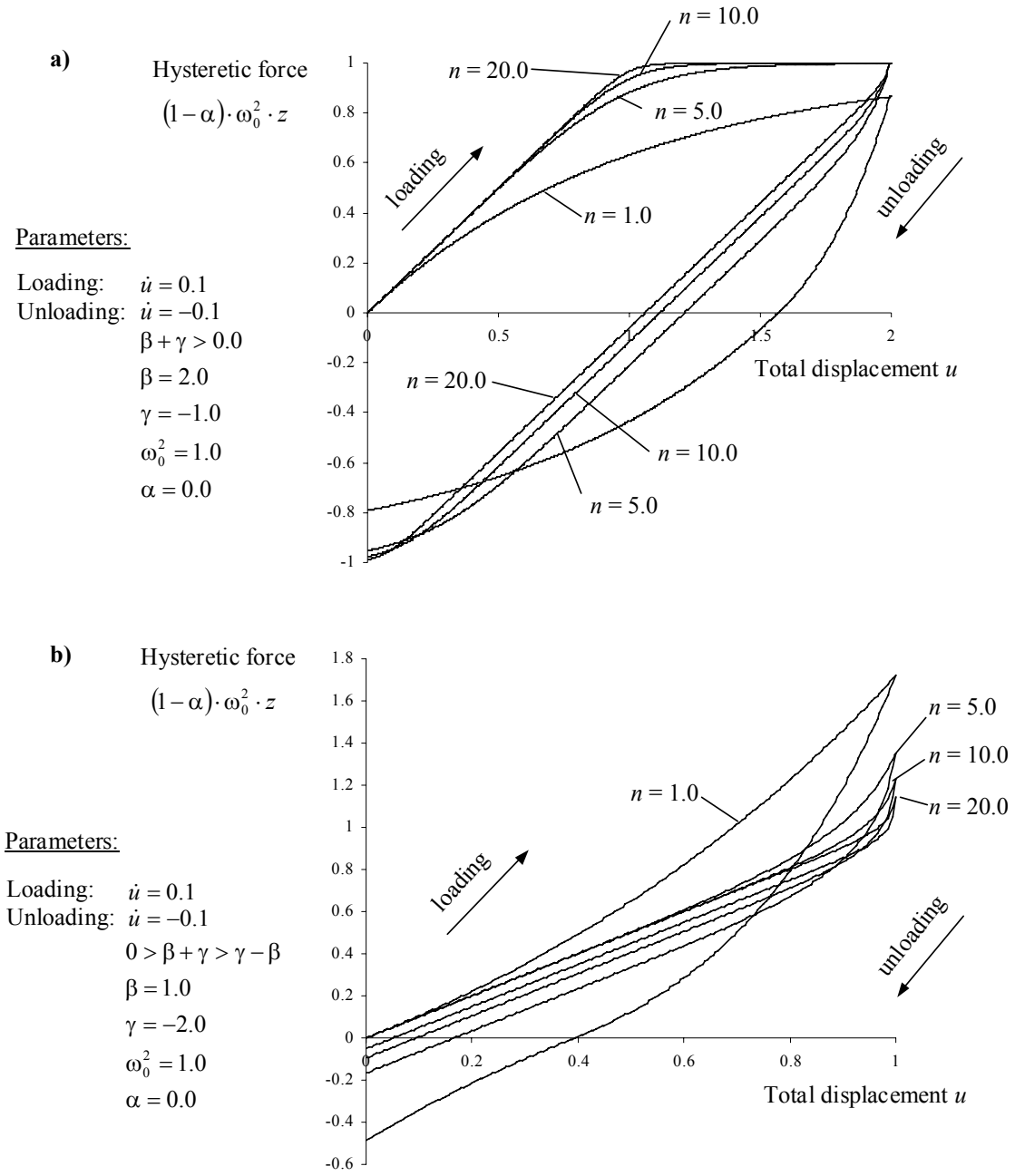


Figure 5.3: a) Hysteretic force versus total displacement, *u*. Effect of increasing *n* on softening hysteresis is shown. All other parameters are kept constant. b) Similar to a) but $\beta$ and $\gamma$ are set to yield a hardening hysteresis.

During loading, the parameter *n* controls the sharpness of the transition from initial slope to the slope of the asymptote, which *z* approaches in a softening hysteresis. For increasing values of *n*, the loading path of a softening hysteresis approaches the ideal elastic-plastic function while the unloading path approaches a straight line (Figure 5.3). In contrast, the effect on hardening hysteresis shapes is quite different as depicted in Figure 5.3. Growing values of *n* cause the hysteresis to narrow and the transition from linear to hardening to sharpen.

*5.2.1.2 Hysteretic Energy*

The hysteretic energy absorption is used by the BWBN model to approximate system degradation (discussed in Section 5.2.1.3). The energy absorbed by the hysteretic element is simply the continuous integral of the hysteretic force, $f_h$, over the total displacement $u$. After some manipulation, the hysteretic energy absorption may be expressed as (Foliente 1993)

$$\varepsilon(t) = \int_{u(0)}^{u(T)} f_h \cdot du = (1.0 - \alpha) \cdot \omega^2 \cdot \int_{u(0)}^{u(T)} z(u,t) \cdot du \cdot \frac{dt}{dt} = (1.0 - \alpha) \cdot \omega^2 \cdot \int_{0}^{T} z(u,t) \cdot \dot{u}(t) \cdot dt \quad (5.13)$$

As depicted in Figure 5.4, the absorbed energy increases exponentially with a linearly increasing forcing function. The periodic increase results from the fact that the total energy (absorbed energy) is computed at each time step, not just the energy enclosed in the hysteresis loop (dissipated energy).

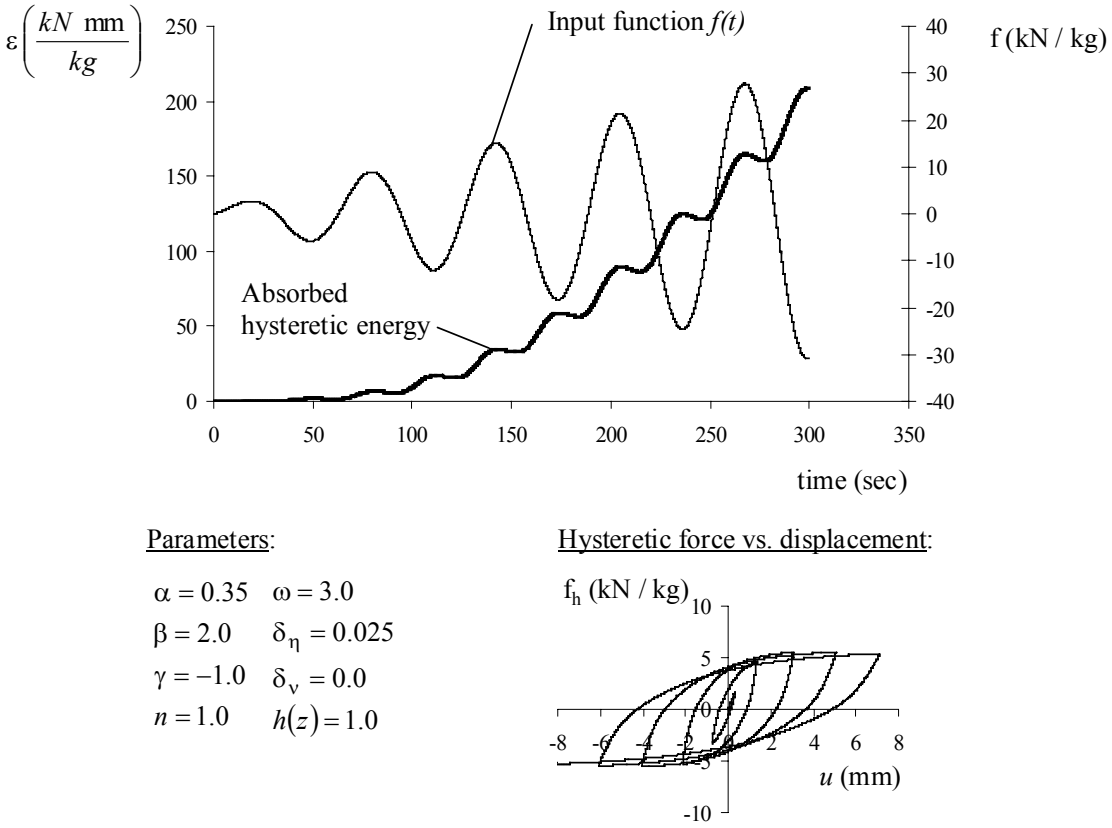


Figure 5.4: Total absorbed hysteretic energy vs. time for the non-pinching BWBN model (h(z) = 1.0). Forcing function, input parameters, and the resulting hysteresis are also shown.

*5.2.1.3 Degradation*

Degradation is easily added to Equation (5.7). The BWBN model approximates response history dependency, or strength (if the input is displacement) and stiffness degradation, by adding two factors to the hysteresis equation. Factor $\eta$ simply reduces the entire hysteretic displacement and hence the hysteretic force, based on absorbed hysteretic energy $\varepsilon(t)$.

$$\dot{z}(t) = \frac{\dot{u}(t) - \left(\beta \cdot |\dot{u}(t)| \cdot |z(t)|^{n-1} \cdot z(t) + \gamma \cdot \dot{u}(t) \cdot |z(t)|^{n}\right)}{\eta} \tag{5.14}$$

Where $\eta$ is the linearly varying function

$$\eta = 1.0 + \delta_{\eta} \cdot \varepsilon(t) \tag{5.15}$$

Other dependencies of $\eta$ may be incorporated if needed, such as a non-linear relationship with $\varepsilon(t)$ or another variable. Note that both hysteretic force and hysteretic stiffness degrade as $\delta_\eta$ increases (Figure 5.5). If force is the input function, and total force versus displacement is considered, then the reduction of the hysteretic force results in total stiffness degradation only, whereas both total strength and total stiffness degrade if displacement is the independent variable. Caused by the exponential energy increase with linearly increasing force, the system degrades nonlinearly and is quite sensitive to $\delta_\eta$ (Figure 5.5).

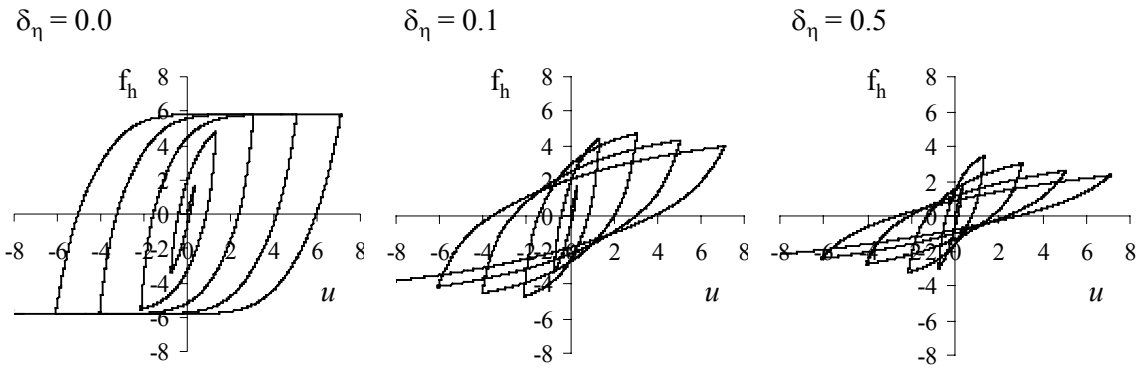


Figure 5.5: System degradation with changing $\delta_\eta$. (Except for $\delta_\eta$,, parameters and input function are same as in Figure 5.4)

In order to incorporate another type of degradation, the BWBN model employs a second factor, $\nu$, with which the hysteresis equation becomes

$$\dot{z}(t) = \frac{\dot{u}(t) - \nu \cdot \left(\beta \cdot |\dot{u}(t)| \cdot |z(t)|^{n-1} \cdot z(t) + \gamma \cdot \dot{u}(t) \cdot |z(t)|^{n}\right)}{\eta} \tag{5.16}$$

Where $\nu$ also varies linearly with $\varepsilon$

$$\nu = 1.0 + \delta_\nu \cdot \varepsilon(t) \tag{5.17}$$

The effect of varying $\delta_\nu$ can be observed in Figure 5.6. An increase in $\delta_\nu$ reduces the total amplitude of the hysteretic force without changing the hysteretic stiffness, essentially capping the hysteretic force at decreasing values. The BWBN solution is even more sensitive to $\delta_\nu$ than $\delta_\eta$.

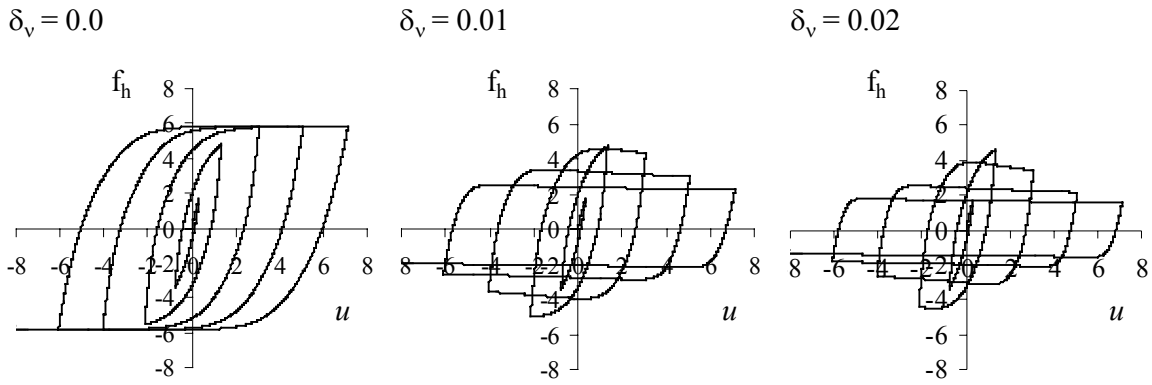


Figure 5.6: System degradation with changing $\delta_v$. (Except for $\delta_v$, parameters and input function are same as in Figure 5.4)

### 5.2.2 Pinching and Slack Model

A simpler pinching function is sought that incorporates pinching as well as slack and slack growth based on displacement amplitude rather than energy dissipation. Furthermore, slack asymmetry needs to be taken into account on grounds that in a multiple-bolt joint there may be more slack in one direction of movement than in the other for any given bolt due to tolerances in bolt hole spacing between members.

The inclusion of slack makes it necessary to modify both the linear element as well as the hysteretic element since the bolt only comes in contact with the wood foundation when the lateral displacement is larger than the slack in the direction of movement. Therefore, the equivalent system modeled changes to the system depicted in Figure 5.7. Viscous damping forces and inertia forces are not slack dependent, presuming that the friction force caused by the slipping bolt in the oversized hole and the abutting member surfaces follows viscous-elastic theory. Hysteretic and restoring force, on the other hand, are zero or close to zero until slack in either direction of movement is overcome.

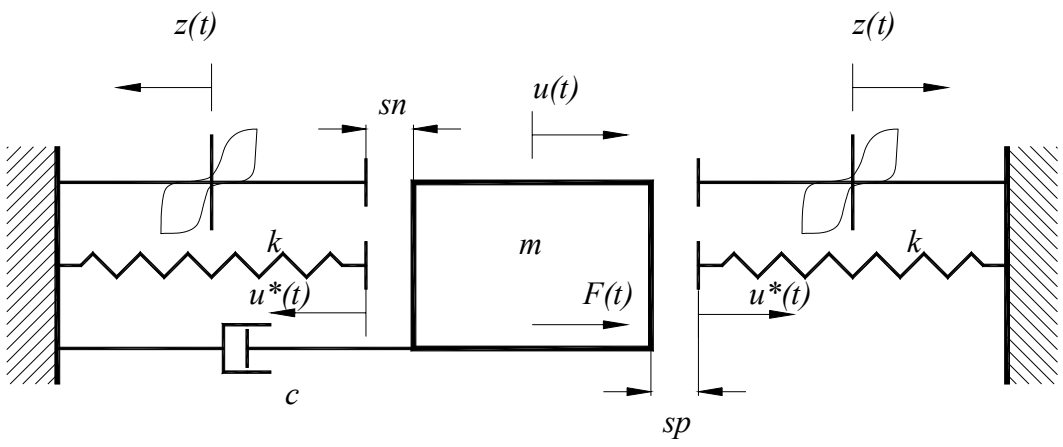


Figure 5.7: Equivalent system described by the modified hysteresis model. *sn* and *sp* denote slack in positive and negative direction of movement, respectively.

Values of *sp* and *sn* are not constant since slack grows when the elastic limit of the wood foundation is exceeded. A relatively simple way to model slack and slack growth is to linearly relate it to the maximum displacement amplitudes (positive and negative) reached before or at time *T*

$$sp = \psi_0 + \delta_\psi \Delta(t) \quad \text{for } \Delta(t) > 0.0 \tag{5.18}$$

$$sn = \psi_0 + \delta_\psi \Delta(t) \quad \text{for } \Delta(t) < 0.0 \tag{5.19}$$

where

$$\Delta(t) = \begin{cases} \text{Global max}\left[u(t)\right]_{t=0}^{T} & \text{if } u(T) \geq 0.0 \\ \text{Global min}\left[u(t)\right]_{t=0}^{T} & \text{if } u(T) < 0.0 \end{cases} \tag{5.20}$$

Parameters $\psi_0$ and $\delta_\psi$ describe initial slack and slack growth, respectively. The increase of $\Delta$ versus the resisted force with an increasing displacing function is revealed in Figure 5.8. It is clear that $\Delta(t)$ is not a continuous function. However, since $\Delta(t)$ is not a variable but a parameter and because it is known at each time step, the model is still fully traceable mathematically.

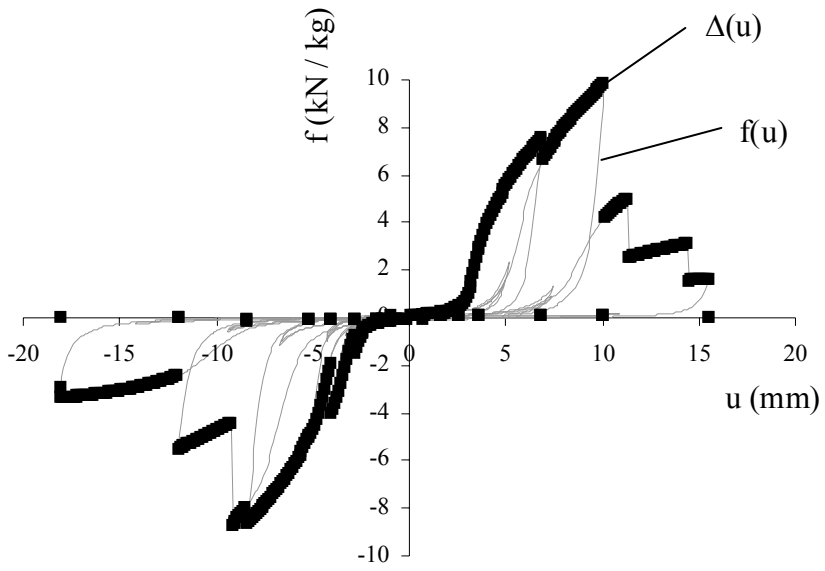


Figure 5.8: Values of *Δ* (square dots) plotted versus total force. Input function is increasing displacing function. The graph shows pre- and post- failure response.

Since pinching represents non-linear behavior, it is straight forward to relate any type of pinching to the hysteretic displacement (Baber and Noori 1986), which in turn is directly proportional to the hysteretic force. Thus, including the pinching function *h(z),* Equation (5.16) becomes

$$\dot{z}(t) = h(z) \cdot \frac{\dot{u}(t) - \nu \cdot \left( \beta \cdot |\dot{u}(t)| \cdot |z(t)|^{n-1} \cdot z(t) + \gamma \cdot \dot{u} \cdot |z(t)|^{n} \right)}{\eta} \tag{5.21}$$

Note, if *h(z)* assumes a value of 1.0, no pinching exists and Equation (5.21) reverts to Equation (5.16). Bearing in mind the formulation of slack growth derived earlier, the basic characteristic of a pinching function for bolted joints in timber may then be described as

$$h(z) = \begin{cases} 0.0 & \text{if} \quad sn \le u \le sp \\ 1.0 & \text{if} \quad u(t) = \Delta(t) \end{cases} \tag{5.22}$$

A simple expression that satisfactorily meets the requirements stated in Equation(5.22) is the inverse of an impulse function (Figure 5.9). The most widely used approximation of a peak impulse function is the bell curve or Gaussian density function. Thus, the pinching function was derived from the bell curve and takes the form

$$h(z) = 1.0 - \zeta \cdot e^{\left( \frac{-(z(t))^2}{\left(\psi_0 + \delta_\psi \cdot |\Delta(t)|\right)^2} \right)} \tag{5.23}$$

for

$$\left\{ \begin{array}{c} 0.0 \le \zeta < 1.0 \\ 0.0 \le \delta_\psi \le 1.0 \\ 0.0 < \psi_0 \end{array} \right\} \tag{5.24}$$

| | | Unit |
|---|---|---|
| $u$ | total displacement of the mass, $m$ | mm |
| $z$ | hysteretic displacement | mm |
| $\Delta$ | global maximum or minimum displacement amplitude at or before time $T$ | mm |
| $\psi_0$ | parameter controlling initial slack | mm |
| $\delta_\psi$ | slack growth parameter | |
| $\zeta$ | parameter determining the level of pinching | |

Although it is mathematically possible, parameter $\zeta$ cannot assume a value of 1.0 because it results in zero hysteretic stiffness and the numeric solution will not yield desired results. The width (or significant pinching region) of the inverse peak of Equation (5.23) is determined by (Figure 5.9)

$$\Omega = \psi_0 + \delta_\psi \cdot |\Delta(t)| \tag{5.25}$$

Expression (5.23) is similar in principle to the one proposed by Baber and Noori (1986) (eq. (4.6)) but different to the extent that it is simplified and allows pinching to be maximum at small displacements and zero dissipated energy. In addition, pinching is now displacement dependent rather than a function of hysteretic energy.

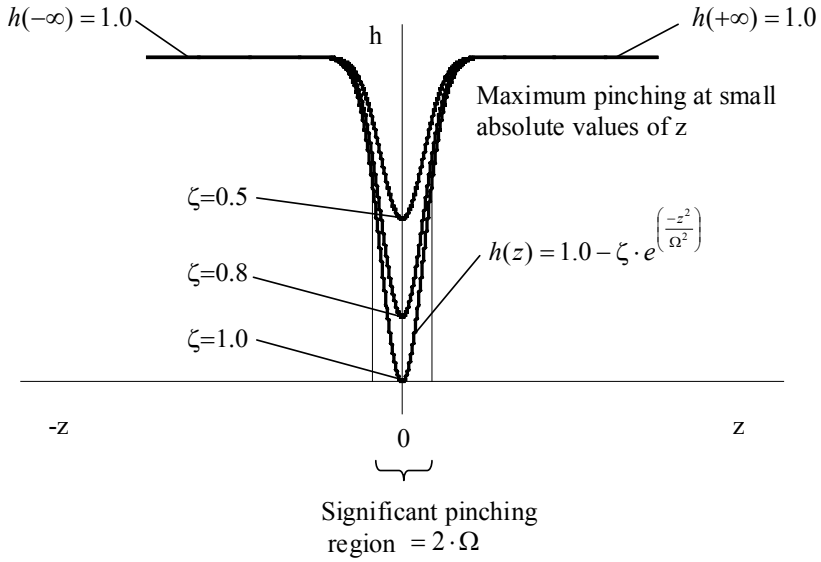


Figure 5.9: Pinching function *h(z)* plotted at various ζ.

The continuous nature of the pinching function produces smooth hysteresis loops with a gradual transition from almost zero stiffness to maximum hysteretic stiffness. In order to allow an equally smooth transition from no-contact to contact of the linear element and in order to increase the influence of the linear restoring force in tandem with the decrease of pinching, the linear restoring force is related to the total joint displacement *u* by (Figure 5.7)

$$f_R(t) = \alpha \cdot \omega^2 \cdot u^*(t) = \alpha \cdot \omega^2 \cdot u(t) \cdot \left( 1.0 - e^{\left( \frac{-(z(t))^2}{(\psi_0 + \delta_\psi \cdot |\Delta(t)|)^2} \right)} \right) \tag{5.26}$$

The part in parentheses of Equation (5.26) is almost identical to Equation (5.23) with the exception that the parameter $\zeta$ is 1.0 and therefore omitted. For a slack system, the restoring force is always zero if total displacement is smaller than slack in any direction. In addition, unlike in the hysteretic equation (Eq. (5.23)), no singularity occurs if the term in parenthesis of Equation (5.26) becomes zero.

### 5.2.3 Complete Hysteresis Model for Slack Systems

Accounting for slack and slack growth in the linear and hysteretic elements, the complete hysteresis model for bolted joints becomes

$$\overbrace{\ddot{u}(t)}^{\text{acceleration}} + \overbrace{2\cdot\xi_0\cdot\omega\cdot\dot{u}(t)}^{\text{velocity}} + \overbrace{\alpha\cdot\omega^2\cdot u(t)\cdot\left(1.0 - e^{\left(\frac{-(z(t))^2}{\left(\psi_0+\delta_\psi\cdot|\Delta(t)|\right)^2}\right)}\right)}^{\text{stiffness and slack}} + \overbrace{(1-\alpha)\cdot\omega^2\cdot z(t)}^{\text{hysteresis}} = \overbrace{f(t)}^{\text{forcing function}} \quad (5.27)$$

where

$$\dot{z}(t) = \left[1.0 - \zeta\cdot e^{\left(\frac{-(z(t))^2}{\left(\psi_0+\delta_\psi\cdot|\Delta(t)|\right)^2}\right)}\right]\cdot\left[\frac{\dot{u}(t) - \nu\cdot\left(\beta\cdot|\dot{u}(t)|\cdot|z(t)|^{n-1}\cdot z(t) + \gamma\cdot\dot{u}\cdot|z(t)|^n\right)}{\eta}\right] \quad (5.28)$$

and

$$\eta = 1.0 + \delta_\eta\cdot\varepsilon(t) \quad (5.29)$$

$$\nu = 1.0 + \delta_\nu\cdot\varepsilon(t) \quad (5.30)$$

$$\varepsilon(t) = (1.0-\alpha)\cdot\omega^2\cdot\int_0^T z(t)\cdot\dot{u}(t)\cdot dt \quad (5.31)$$

| | | Unit |
|---|---|---|
| $\omega$ | pseudo-natural frequency of the non-linear system | rad/sec $10^6$ |
| $f(t)$ | force function (mass normalized) | kN/kg |
| $t$ | time | sec |
| $\xi$ | viscous damping ratio of the linear system | |
| $u$ | total displacement of the mass, $m$ | mm |
| $z$ | hysteretic displacement | mm |
| $\alpha$ | rigidity ratio | |
| $\delta_\nu$ | degradation parameter | |
| $\delta_\eta$ | degradation parameter | |
| $\beta, \gamma, n$ | parameters describing shape and amplitude of hysteresis $1.0 \le n$ | |
| $\Delta$ | global maximum or minimum displacement amplitude at or before time $T$ | mm |
| $\psi_0$ | parameter controlling initial slack | mm |
| $\delta_\psi$ | slack growth parameter | |
| $\zeta$ | parameter determining the level of pinching | |

The model is now capable of describing smooth hysteresis loops for slack systems (Figure 5.10). Moreover, the modified model accounts for asymmetric loading, which causes the slack to grow more in one displacement direction than in the other. In addition, it is possible to assign a random

slack size to either direction of movement, which allows the stochastic modeling of variability in slack of multiple bolt joints due to manufacturing tolerances. The total number of parameters that need to be identified is reduced to eleven.

**a) Total force vs. displacement**

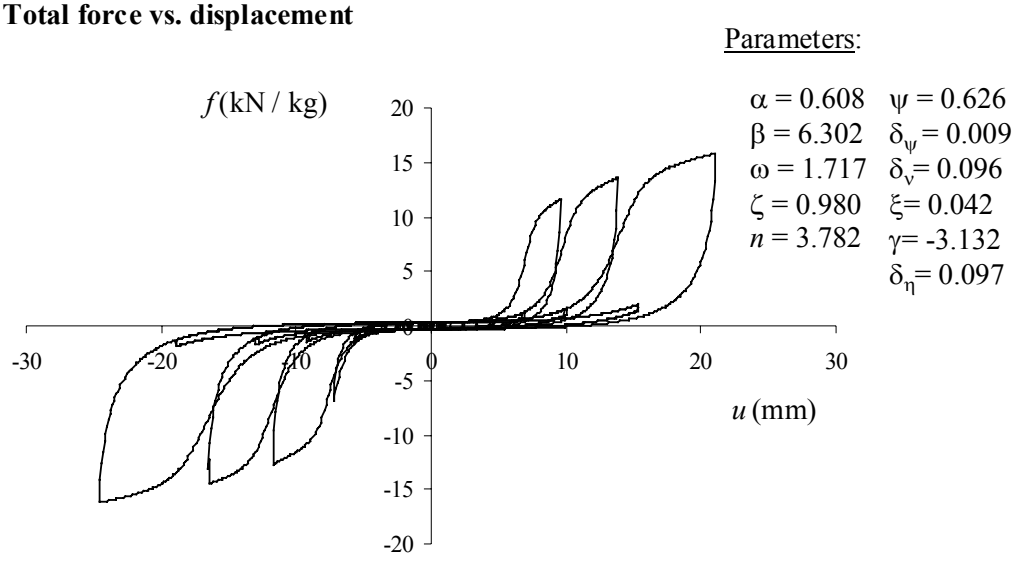


**b) Hysteretic force vs. displacement**

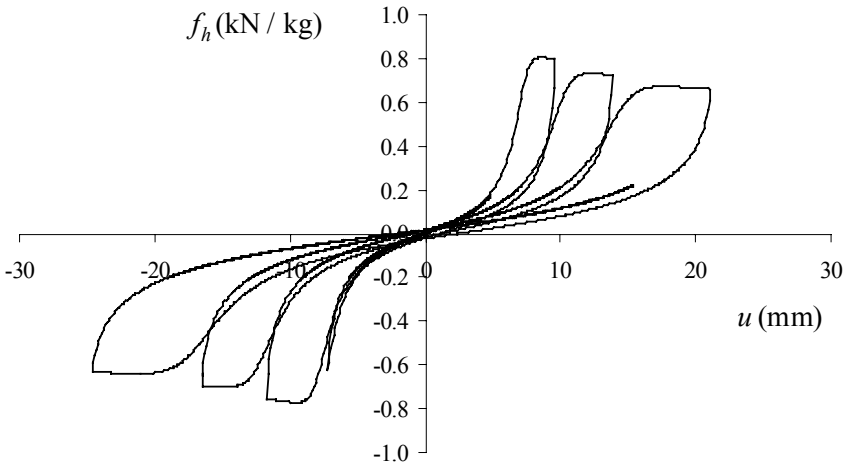


Figure 5.10: Hysteresis produced by the modified model: a) Plot of total force *f* versus displacement *u* with large slack region. b) Plot of hysteretic force, $f_h$, versus displacement *u*. Input function was increasing displacing function.

## 5.3 Model Solving

In Equations (5.27) to (5.31) all derivatives appear in the first power and variables vary with time at highly different rates. Hence, the modified hysteresis model constitutes a stiff set of linear ordinary differential equations (ODE), which can be solved numerically using Gear's backward differentiation formulas (Gear 1971). While there exists an abundance of numerical methods to solve sets of stiff ODEs, the most widely used solver is the Livermore Solver for Ordinary Differential Equations (LSODE), which is part of the ODEPACK User Interface Standard (Hindmarsh 1983). ODEPACK can be downloaded free of charge in FORTRAN from the Netlib Repository, a collection of mathematical software (www.netlib.org). LSODE solves a wide range of ODEs including stiff systems for which it uses the Gear Method and it is capable of internally computing the full Jacobian matrix. Moreover, input functions such as displacing or forcing functions do not have to be continuous functions. Instead discrete data points can be read in from an external file. Thanks to a very detailed user manual that is included in the comment lines of the main subroutine, the standardized user interface of LSODE is easily integrated in other programs written by the user. LSODE was incorporated into MULTBOLT.

### 5.3.1 First-Order Form

LSODE requires the user to convert the system of ODEs into first-order form to obtain an array of first-order ODEs (Hindmarsh 1983)

$$\frac{dy}{dt} = f(t, y) \tag{5.32}$$

where $y$ is a vector containing the set of ODEs and $f$ is a vector-valued function of $t$ and $y$. Subsequently, using the relation (Baber and Noori 1985, Foliente 1993)

$$\begin{Bmatrix} y_1(t) \\ y_2(t) \\ y_3(t) \\ y_4(t) \end{Bmatrix} = \begin{Bmatrix} u(t) \\ \dot{u}(t) \\ z(t) \\ \varepsilon(t) \end{Bmatrix} \tag{5.33}$$

the modified hysteresis model presented in Equations (5.27) to (5.31) may be rearranged and manipulated to yield (for clarity, time dependencies are omitted)

$$\dot{y}_1 = y_2 \tag{5.34}$$

$$\dot{y}_2 = -\alpha \cdot \omega^2 \cdot y_1 \cdot \left( 1.0 - e^{\left( \frac{-y_3{}^2}{(\psi_0 + \delta_\psi \cdot |\Delta|)^2} \right)} \right) - 2.0 \cdot \xi_0 \cdot \omega \cdot y_2 - (1.0 - \alpha) \cdot \omega^2 \cdot y_3 + f \tag{5.35}$$

$$\dot{y}_3 = \left[ 1.0 - \zeta \cdot e^{\left( \frac{-y_3{}^2}{(\psi_0 + \delta_\psi |\Delta|)^2} \right)} \right] \cdot \left[ \frac{y_2 - (1.0 + \delta_\nu \cdot y_4) \cdot \left( \beta \cdot |y_2| \cdot |y_3|^{n-1} \cdot y_3 + \gamma \cdot y_2 \cdot |y_3|^n \right)}{1.0 + \delta_\eta \cdot y_4} \right] \tag{5.36}$$

$$\dot{y}_4 = (1.0 - \alpha) \cdot \omega^2 \cdot y_2 \cdot y_3 \tag{5.37}$$

### 5.3.2 Multiple Bolt Solution

The general modeling of multiple-bolt joints requires a different set of parameter values for each individual fastener. The possibility to vary parameters for each bolt separately, allows the stochastic modeling of material property variation around each bolt. Furthermore, as elaborated in previous sections, the load or displacement among the fasteners in a multiple-bolt joint is not shared equally due to material deformations and slack. Consequently, for load or displacement input, each bolt experiences a unique loading function and displacing function, respectively. Therefore, a different hysteresis model must be solved for each fastener. But since it is desired to allow the number of fasteners in a row to change, the number of differential equations to be solved by the solver is not constant. The problem is resolved by use of arrays and embedment of LSODE into a dynamic loop. This is possible because LSODE permits dynamic size of the ODE system and the input of ODEs in array form. For a multiple bolt-joint the system of ODEs changes to

$$\dot{y}_{(i)} = y_{(i+1)} \tag{5.38}$$

$$\dot{y}_{(i+1)} = -\alpha_{(j)} \cdot \omega^2(j) \cdot y_{(i)} \cdot \left( 1.0 - e^{\left( \frac{-y_{(i+2)}{}^2}{\left( \psi_{0(j)} + \delta_{\psi(j)} \cdot \left| \Delta_{(j)} \right| \right)^2} \right)} \right) - \tag{5.39}$$

$$2.0 \cdot \xi_{0(j)} \cdot \omega_{(j)} \cdot y_{(i+1)} - \left(1.0 - \alpha_{(j)}\right) \cdot \omega^2(j) \cdot y_{(i+2)} + f_{(j)}$$

$$\dot{y}_{(i+2)} = \left[ 1.0 - \zeta \cdot e^{\left( \frac{-y_{(i+2)}{}^2}{\left( \psi_{0(j)} + \delta_{\psi(j)} \cdot \left| \Delta_{(j)} \right| \right)^2} \right)} \right] \cdot \tag{5.40}$$

$$\left[ \frac{y_{(i+1)} - \left(1.0 + \delta_{\nu(j)} \cdot y_{(i+3)}\right) \cdot \left( \beta_{(j)} \cdot \left| y_{(i+1)} \right| \cdot \left| y_{(i+2)} \right|^{n-1} \cdot y_{(i+2)} + \gamma_{(j)} \cdot y_{(i+1)} \cdot \left| y_{(i+2)} \right|^n \right)}{1.0 + \delta_{\eta(j)} \cdot y_{(i+3)}} \right]$$

$$\dot{y}_{(i+3)} = \left(1.0 - \alpha_{(j)}\right) \cdot \omega^2(j) \cdot y_{(i+1)} \cdot y_{(i+2)} \tag{5.41}$$

where all parameters are stored in arrays of size *nbolt, y* and *ydots* are stored in arrays of size *4*nbolt* and

$$j = 1,2,3,\cdots,nbolt \tag{5.42}$$

and

$$i = 1,5,9,\cdots,\left(4 \cdot nbolt\right) \tag{5.43}$$

The variable *nbolt* denotes the number of bolts in a row.

To solve the model for displacement, that is, input function is a forcing function, a discrete value of $f_{(j)}$ is read in for each bolt and time interval at the end of which a solution is desired. Since the solver chooses step size automatically, the size of the time interval is not necessarily equal the internal step size of the solver. The solution at the end of each time interval for which a new $f_{(j)}$ was input is an array of size *4*nbolt* storing $y_1$, $y_2$, $y_3$, $y_4$ for each bolt.

Most cyclic tests on bolted joints are displacement controlled, however, not least because failure is much easier to monitor. It is therefore desirable to choose displacement as the independent variable and solve for force. Since the displacing function is already known, the derivative of the displacing function – the velocity function – and of course its derivative – the acceleration function – are also known and the hysteresis model can be solved without difficulty. However, to keep the required first-order form, Equation (5.39) is taken out of the set of ODEs so that only three remain. Once $y_3$, is computed by the solver, all y(i)'s are defined and it is straight forward to compute $f_{(j)}$ from Equation (5.39). The derivatives of a discrete list of numbers such as a displacing function record stored in a file can obviously only be computed if the data acquisition frequency is known. The most common way to differentiate numerically is by Euler differentiation

$$\frac{\delta y}{\delta t} \approx \frac{y(t+\Delta t)-y(t)}{\Delta t} \quad \text{for} \quad \Delta t \to 0 \tag{5.44}$$

However, depending on the size of the time interval, better accuracy may be obtained with the central difference method

$$\frac{\delta y}{\delta t} \approx \frac{y(t+\Delta t)-y(t-\Delta t)}{2\cdot\Delta t} \quad \text{for} \quad \Delta t \to 0 \tag{5.45}$$

But at small time intervals rounding error may exceed truncation error.

### 5.3.3 Remarks

Computing time to solve the model and numeric noise are greatly reduced if both force and displacement are in the same order of magnitude. For instance, for bolted joints, the units [kN] and [mm] are a good choice. For the single-bolt joints tested for this study, maximum load ranged between roughly 10 and 40 kN and was reached at displacements between 5 and 25 mm. Efficient computing becomes especially important if a randomized system identification technique is used to identify the parameters.

The LSODE solver employs user-specified relative and absolute error control. Satisfactory results were achieved with relative error control turned off and absolute error kept constant for all *y*s at $10^{-12}$ (unit depends on the *y* in question).

## 5.4 Hysteresis Model Calibration

Recall that the hysteresis model describes the load displacement relation of the individual fastener. Therefore, it must be calibrated to cyclic test results of single-bolt joints where the two principal geometries, bolt diameter and member thickness, are the same as for the multiple-bolt joint whose performance is to be predicted, provided that minimum edge and end distances are not violated. While this may seem like a limitation, it only exists until there is enough data available to allow stochastic predictions of hysteresis parameters based on bolt diameter, member thickness and specific gravity.

Because the hysteresis model is derived from a physical system, it is, if properly calibrated, applicable to random input functions. This is important since each fastener in a multiple bolt joint experiences a unique displacing or loading function due to material deformations. Likewise, it should be possible to predict multiple-bolt response to random displacement inputs such as earthquake records.

At this point, model calibration is essentially curve fitting to experimental data. Curve fitting is an optimization problem in that the difference between model output and test result needs to be minimized. Derived from the fact that one of the objectives of this research was to predict failure and given that true seismic excitation of structures is displacement driven, calibration tests were also displacement controlled. Hence, the common input function was a displacing function and the hysteresis model was fit to load output. To fit the model to experimental data, a systematic parameter search routine – or system identification method – was developed. Details of the parameter estimation process are described in Chapter 6.